Calculated Epithelial/Absorbed Power Density for Exposure From Antennas at 10-90 GHz: Intercomparison Study Using a Planar Skin Model

Kun Li, Sachiko Kodera, Dragan Poljak, Yinliang Diao, Kensuke Sasaki, Anna Šušnjara, Alexander Prokop, Kenji Taguchi, Jingtian Xi, Shuai Zhang, et al.

IEEE Access
Multidisciplinary | Rapid Review | Open Access Journal

Received 30 November 2022, accepted 16 January 2023, date of publication 20 January 2023, date of current version 25 January 2023.

Digital Object Identifier 10.1109/ACCESS.2023.3238582

RESEARCH ARTICLE

Calculated Epithelial/Absorbed Power Density for Exposure From Antennas at 10–90 GHz: Intercomparison Study Using a Planar Skin Model

KUN LI[1], (Member, IEEE), SACHIKO KODERA[2], (Member, IEEE), DRAGAN POLJAK[3], (Senior Member, IEEE), YINLIANG DIAO[4], (Member, IEEE), KENSUKE SASAKI[5], (Member, IEEE), ANNA ŠUŠNJARA[3], (Member, IEEE), ALEXANDER PROKOP[6], (Senior Member, IEEE), KENJI TAGUCHI[7], (Member, IEEE), JINGTIAN XI[8], (Member, IEEE), SHUAI ZHANG[9], (Senior Member, IEEE), MING YAO[9], (Graduate Student Member, IEEE), GIULIA SACCO[10], (Member, IEEE), MAXIM ZHADOBOV[10], (Senior Member, IEEE), WALID EL HAJJ[11], (Member, IEEE), AND AKIMASA HIRATA[2], (Fellow, IEEE)

[1]Faculty of Engineering and Design, Kagawa University, Takamatsu 761-0396, Japan
[2]Department of Electrical and Mechanical Engineering, Nagoya Institute of Technology, Nagoya 466-8555, Japan
[3]Faculty of Electrical Engineering, Mechanical Engineering and Naval Architecture, University of Split, 21000 Split, Croatia
[4]College of Electronic Engineering, South China Agricultural University, Guangzhou 510642, China
[5]National Institute of Information and Communications Technology, Tokyo 184-8795, Japan
[6]Dassault Systèmes SIMULIA, 64293 Darmstadt, Germany
[7]Department of Electrical and Electronic Engineering, Kitami Institute of Technology, Kitami 090-8507, Japan
[8]Foundation for Research on Information Technologies in Society (IT'IS), 8004 Zurich, Switzerland
[9]Department of Electronic Systems, Aalborg University, 9220 Aalborg, Denmark
[10]Institut d'Électronique et des Technologies du numéRique (IETR), CNRS, UMR 6164, University of Rennes 1, 35000 Rennes, France
[11]Wireless Test and Certification Center, Intel, Intel Corporation, 06600 Antibes, France

Corresponding author: Kun Li (li.kun@kagawa-u.ac.jp)

ABSTRACT International organizations have collaborated to revise standards and guidelines for human protection from exposure to electromagnetic fields. In the frequency range of 6–300 GHz, the permissible spatially averaged epithelial/absorbed power density, which is primarily derived from thermal modeling, is considered as the basic restriction. However, for the averaging methods of the epithelial/absorbed power density inside human tissues, only a few groups have presented calculated results obtained using different exposure conditions and numerical methods. Because experimental validation is extremely difficult in this frequency range, this paper presents the first intercomparison study of the calculated epithelial/absorbed power density inside a human body model exposed to different frequency sources ranging from 10–90 GHz. This intercomparison aims to clarify the difference in the calculated results caused by different numerical electromagnetic methods in dosimetry analysis from 11 research groups using planar skin models. To reduce the comparison variances caused by various key parameters, computational conditions (e.g., the antenna type, dimensions, and dielectric properties of the skin models) were unified. The results indicate that the maximum relative standard deviation (RSD) of the peak spatially averaged epithelial/absorbed power densities for one- and three-layer skin models are less than 17.49% and 17.39%, respectively, when using a dipole antenna as the exposure source. For the dipole array antenna, the corresponding maximum RSD increases to 32.49% and 42.55%, respectively. Under the considered exposure scenarios, the RSD in the spatially averaged epithelial/absorbed power densities decrease from 42.55% to 16.7% when the frequency is increased from 10–90 GHz. Furthermore, the deviation from the two equations recommended by the exposure guidelines

The associate editor coordinating the review of this manuscript and approving it for publication was Sandra Costanzo.

for deriving the spatially averaged epithelial/absorptive power density is mostly within 1 dB. The fair agreement in the intercomparison results demonstrates that the variances of the spatially averaged epithelial/absorbed power densities calculated using planar skin models are marginal.

INDEX TERMS Dosimetry modeling, electromagnetic field, epithelial/absorbed power density, millimeter wave exposure, standardization, skin model.

I. INTRODUCTION

Owing to the development of various wireless systems, research on the protection of humans exposed to electromagnetic fields (EMFs) has attracted considerable attention [1], [2], [3], [4]. In 2019 and 2020, the IEEE International Committee on Electromagnetic Safety (ICES) Technical Committee (TC) 95 and the International Commission on Non-Ionizing Radiation Protection (ICNIRP) revised the exposure standards and guidelines, respectively, to prescribe the exposure limits for people in restricted environments/occupational exposure and for unrestricted environments/general public exposure conditions [5], [6].

In the revised standard/guidelines, the two-tier approach is used, similar to the previous versions. The epithelial/absorbed power density (hereafter referred as APD) is used as a new internal physical quantity to set the dosimetric reference limit (DRL) or basic restriction (BR), which is derived from the operational threshold of adverse health effects, considering the safety or reduction factor in the frequencies from 6–300 GHz. These DRL or BR were derived based on thermal modeling [7], [8], [9], [10], [11], [12], which provides a high degree of protection against dominant adverse health effects of exposure, that is, localized temperature elevation on the surface of human skin tissue. To correlate well with the local maximum temperature increase, it is suggested that the APD be averaged over an area of 4 cm^2 from 6–300 GHz. Above 30 GHz, a smaller spatial averaging area of 1 cm^2 should also be considered to account for possible narrow-beam exposure scenarios. For this averaging area, the limit was relaxed by a factor of 2. Conversely, the permissible external exposure reference level (ERL) [5] or reference level (RL) [6], that is, the incident power density (IPD) in free space, which is derived from the APD, has been prescribed conservatively. Based on the exposure guidelines/standards, the IPD should be averaged over an area of 4 cm^2 for frequencies ranging from 6–300 GHz. For frequencies higher than 30 GHz, additional criteria of the IPD averaged over 1 cm^2 are given with a relaxation of ERL/RL by a factor of two for local beam-like exposures, similar to those of the spatial average of the APD.

Dosimetric studies for both plane-wave [13], [14], [15], [16], [17], [18], [19], [20], [21] and antenna source exposures [22], [23], [24], [25], [26], [27], [28], [29], [30], [31], [32], [33], [34], [35], [36], [37], [38], [39] were conducted to determine the relationship between the power densities and resultant surface temperature elevation above 6 GHz. Subcommittee 6 of the IEEE ICES TC95 reported on a guide for defining the spatial average of IPD to correlate surface temperature elevation [40]. Using intercomparison from established working groups in dosimetry analysis using various skin and antenna models, the deviations of the heating factors of the spatially averaged IPDs were insignificant [41], including the oblique incidence angle effects caused by phased array antennas [42]. In comparison with the IPD outside human tissue, however, the APD, which is closely correlated with the superficial heating of human tissue, has not been studied sufficiently and to a greater extent. Only a few groups computed the APD and resultant temperature rise at frequencies greater than 6 GHz using different exposure conditions and methods [43], [44], [45], [46], [47]. Considering different important factors (e.g., the antenna type (size), frequency, separation distance from the radiation source, averaging area, and tissue electrical parameters), it is worthwhile to further discuss and clarify the appropriate schemes for the spatial average of the APD in conventional planar models and in non-planar and complex irregular human tissue models.

Under Subcommittee 6 of the IEEE ICES TC95, a new working group (WG) was established, which aims to study and quantify the effects of different schemes on the spatial average of the APD above 6 GHz. The cause of the variances of the numerical calculations in the dosimetry analyses will be evaluated through an objective comparison of the computation results from participating organizations using their proper assessment methods and average schemes with various body and antenna models. This intercomparison of the specific absorption rate (SAR) has been conducted for standardization in frequency bands of a few GHz [48]. This is because the measurement of the field strength in biological bodies is difficult; thus, a computational approach is often conducted. Additionally, for exposure at higher frequencies (particularly above 6 GHz, where the penetration depth is below approximately 1 cm), precise measurement in the depth direction becomes extremely difficult.

The WG task for the average scheme and assessment method of the spatially averaged APD is divided into three phases:

- intercomparison of spatially averaged APD using conventional planar models
- appropriate average schemes using non-planar shaped models (e.g., cylinder or sphere)
- ultimate challenge of the complex irregular voxel model of realistic human tissue, including thermal analysis

To evaluate the deviation of the spatially averaged APD caused by the numerical calculation method of each research

TABLE 1. Exposure scenarios.

Antenna type	Skin Model	Frequency (GHz)	Distance (mm)
$\lambda/2$ dipole, 4×4 dipole array	one-layer, three-layer	10	5, 10, 15
		30	5, 10, 15
		90	2, 5, 10

organization, a traditional planar skin model with unified computational conditions was utilized for the first step of the intercomparison, as mentioned above. This study computed the spatially averaged IPD and APD at the skin surface from 10–90 GHz using computational approaches with unified body and antenna models. An intercomparison of the numerical calculation variances from different research organizations using their simulation codes and commercial electromagnetic (EM) solvers was performed.

II. ANALYTICAL MODEL AND METHOD

A. EXPOSURE SCENARIOS

Eleven different organizations collaborated to conduct this study: Nagoya Institute of Technology (NITech), South China Agricultural University (SCAU), Kagawa University (Kagawa Univ.), Aalborg University (AAU), University of Split (UniSplit), National Institute of Information and Communications Technology (NICT), Kitami Institute of Technology (KITech), Institut d'Électronique et des Technologies du numéRique (IETR), Foundation for Research on Information Technologies in Society (IT'IS), Dassault Systèmes SIMULIA (3DS), and Intel Corporation (Intel). Table 1 presents an overview of the scenarios evaluated numerically by participating organizations. As presented in the table, a separation distance between the antenna and skin surface ranging within 5–15 mm was considered for frequencies of 10 and 30 GHz. At 90 GHz, the separation distances were set from 2–10 mm for the extreme near-field exposure conditions of interest at higher frequencies. Nonetheless, in most wireless device application scenarios, the antenna was not located close to the body to such a separation distance. All the conditions presented in this study clarify the variances in spatially averaged APD computed by different research organizations.

The antenna and planar skin models for the numerical simulations used by different organizations are shown in Fig. 1. As suggested in the discussion of the WG under Subcommittee 6 of the IEEE ICES TC95, a single half-wavelength dipole antenna and a 4×4 dipole antenna array were used in this intercomparison study. The half-wavelength dipole was modeled as a perfect electric conductor. Dipoles were designed at 10, 30, and 90 GHz by each research organization. For most research organizations, the antenna was resonated with an adjusted length to obtain the maximum radiation power emitted from the antenna to the extent possible.

Table 2 summarizes the dipole lengths used by each organization. For the 4×4 dipole antenna arrays, almost the same length (Table 2) was used by the corresponding organization

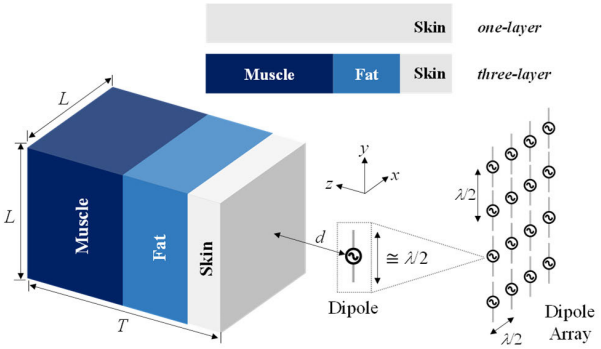

FIGURE 1. Antenna and skin models for dosimetry analysis.

TABLE 2. Lengths of dipole antenna elements for each organization.

Org.	10 GHz (mm)	30 GHz (mm)	90 GHz (mm)
O1	13.75	4.25	1.25
O2	13.5	4.75	1.5
O3	13.6	4.4	1.5
O4	12.6	4.11	1.46
O5	15.0	5.0	1.67
O6	13.75	4.625	1.55
O7	14.5	4.75	1.5
O8	15.0	5.0	1.67
O9	13.6	4.53	1.51
O10	15.0	5.0	1.67
O11	13.49	4.57	1.52

Abbreviations: Organization (Org.).

of the dipole element in the array. The separation distance between the feeding points of any two adjacent dipole elements is $\lambda/2$, where λ is the free-space wavelength. For both dipole and dipole arrays, the total antenna input power was normalized to 10 mW representing a typical power level of mobile devices in the considered frequency range, as in the previous WG [40], [41].

On the other hand, a one-layer skin model and stratified models composed of skin, fat, and muscle layers were employed in this study for dosimetry analysis (Fig. 1). The dimensions of the skin models were $L \times L \times T$ (mm^3; Table 3). The dielectric properties of the tissues obtained by a four-Cole–Cole dispersion model [49], [50], [51] were employed. The electrical parameters for each tissue layer in the skin model are summarized in Table 4.

Table 5 summarizes the numerical techniques used to evaluate the IPD in free space and the APD inside the simplified human tissue models. The spatial resolutions used in each organization were also summarized. The finite-difference time-domain (FDTD) [51] method was adopted by six organizations that used their own developed in-house codes. In

TABLE 3. Dimension and thicknesses of skin models at each frequency.

Skin model	Dimension	10 GHz	30 GHz	90 GHz
one-layer	L (mm)	200	150	60
	T (mm)	100	75	30
three-layer	L (mm)	100	50	50
	T_{skin} (mm)	1.5	1.5	1.5
	T_{fat} (mm)	4.0	4.0	4.0
	T_{muscle} (mm)	14.5	14.5	14.5

TABLE 4. Dielectric properties for skin models.

Skin model	Tissue	10 GHz		30 GHz		90 GHz	
		σ (S/m)	ε_r	σ (S/m)	ε_r	σ (S/m)	ε_r
one-layer	Skin	8.48	32.41	27.31	16.63	41.94	6.83
three-layer	Skin	8.48	32.41	27.31	16.63	41.94	6.83
	Fat	0.59	4.60	1.79	3.64	3.41	2.93
	Muscle	10.63	42.76	35.49	23.16	60.72	9.30

TABLE 5. Numerical method and spatial resolution (Δ) for numerical simulation by each organization.

Org.	Method	10 GHz (mm)	30 GHz (mm)	90 GHz (mm)
O1	FDTD	0.25	0.25	0.05
O2	FDTD	0.5	0.25	0.1
O3	FDTD	0.2	0.2	0.05
O4	FIT	0.25	0.1-0.2	0.01-0.05
O5	GB-IBEM	0.25	0.25	0.25
O6	FDTD	0.25	0.125	0.05
O7	FDTD	0.5	0.25	0.1
O8	FEM	0.014-15.404	0.007-5.557	0.002-1.874
O9	FDTD	0.25-0.05	0.1-0.05	0.0125-0.05
O10	TLM	0.15-1.65	0.1-0.55	0.0333-0.183
O11	FEM	0.5	0.5	0.1

addition to the FDTD methods, the Galerkin-Bubnov indirect boundary element method (GB-IBEM) [53], finite integration technique (FIT) [54], finite element method (FEM) [55], and transmission line method (TLM) [56] have been used separately by other research organizations. It should be noted that the FIT, FEM, and TLM methods used by O4, O8, and O10, respectively, are the three different EM-solvers from commercial simulation software. The other group (O11) that used the FEM method was performed using different types of commercial software. Therefore, this study first covered almost all the commonly used methods of EM simulation for dosimetry analysis without the duplication of commercial software and code. This enables the provision of very neutral and representative intercomparison results to determine the deviation of the calculated APD caused by different numerical methods.

First, the IPDs in free space were calculated without the presence of the body to clarify the influence of the different algorithms on the EM calculations of the antenna near-field. Similar to the previous WG, two definitions of the spatial-average incident power density (*s*IPD), i.e., the normal ($s\text{IPD}_\text{n}$) and norm ($s\text{IPD}_\text{tot}$) component of the time-averaged power density for the EMF, were examined in the absence of the human body (Eqs. (6) and (7) in [41]). The spatial-average APD (*s*APD) in the tissue was calculated for the modeling scenario using the simplified human block model. As recommended in the ICNIRP-2020 exposure guidelines [6], two general equations for deriving the sAPD were employed by each organization, which are expressed by the following formulae:

$$s\text{APD}\,(\boldsymbol{r}) = \frac{1}{A}\iint_A \int_0^{z_{max}} \sigma\,(\boldsymbol{r})\,|\boldsymbol{E}\,(\boldsymbol{r})|^2\,dzds, \tag{1}$$

$$s\text{APD} = \frac{1}{A}\iint_A \text{Re}\left(\boldsymbol{E}\,(\boldsymbol{r}) \times \boldsymbol{H}^*\,(\boldsymbol{r})\right)\cdot d\boldsymbol{s}, \tag{2}$$

where $\boldsymbol{E}$ and $\boldsymbol{H}$ indicates the effective values of the complex electric and magnetic fields inside the body surface, respectively; * denotes the complex conjugate; z_{max} is the depth where the EMF is negligibly small in respect to that at the skin surface; $\boldsymbol{r}$ denotes the position vector; and $d\boldsymbol{s}$ is the integral variable vector whose direction is normal to the integral area A on the body surface (x-y plane at $z = 0$). Because only the planar skin model was considered in this paper, the averaging areas in Eqs. (1) and (2) were averaged over a cubic volume and square area of the flat body surface, respectively, corresponding to the average area of the *s*IPDs.

III. INTERCOMPARISON RESULTS

The intercomparison results in terms of the peak spatial-average IPD and APD (*ps*IPD and *ps*APD) using different antennas are presented in this section. The $ps\text{IPD}_\text{n}$, $ps\text{IPD}_\text{tot}$, and *ps*APD were averaged over an area of $A = 4$ cm^2 and $A = 1$ cm^2 at 10–90 GHz.

A. COMPARISON OF PEAK SPATIAL-AVERAGE INCIDENT POWER DENSITY

Figures 2 and 3 show the results of *ps*IPD as a function of the antenna-to-skin separation distance d exposed to the single half-wavelength dipole or 4 × 4 dipole array antenna for the exposure scenarios in Table 1, respectively. The solid lines indicate the $ps\text{IPD}_\text{n}$, whereas the dashed lines denote the $ps\text{IPD}_\text{tot}$ when $A = 1$ cm^2. The dash-dotted and dotted lines represent the corresponding results for $A = 4$ cm^2.

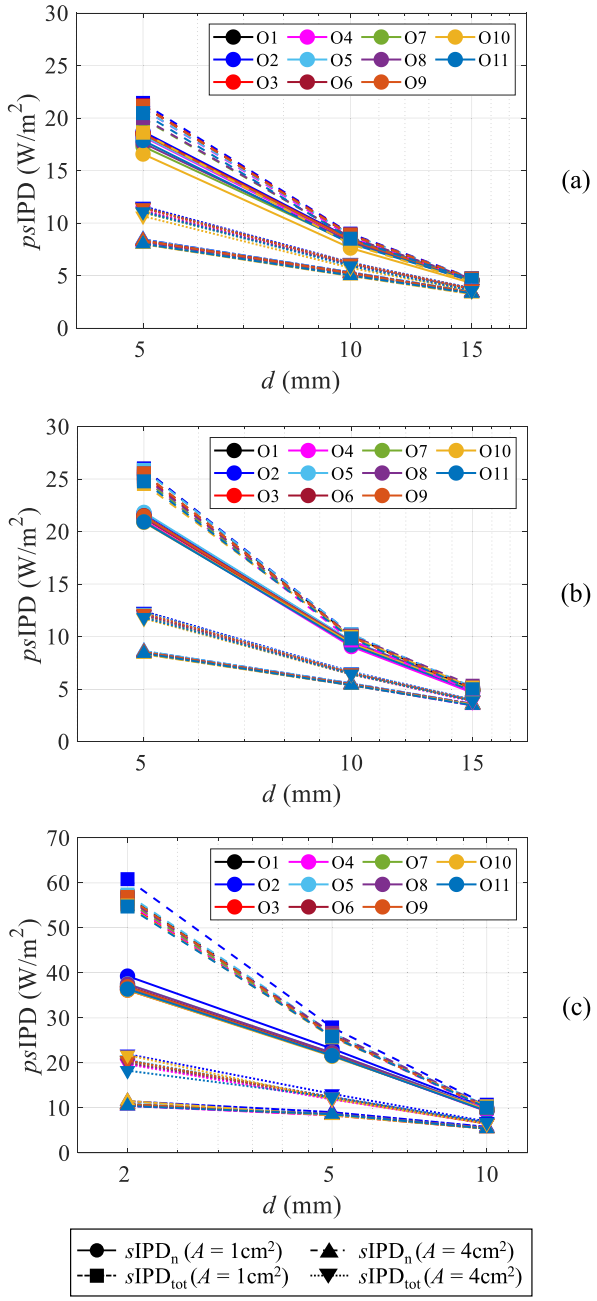

FIGURE 2. Spatially averaged incident power densities as a function of the antenna-to-skin separation distance for half-wavelength dipoles at frequencies of (a) 10, (b) 30, and (c) 90 GHz.

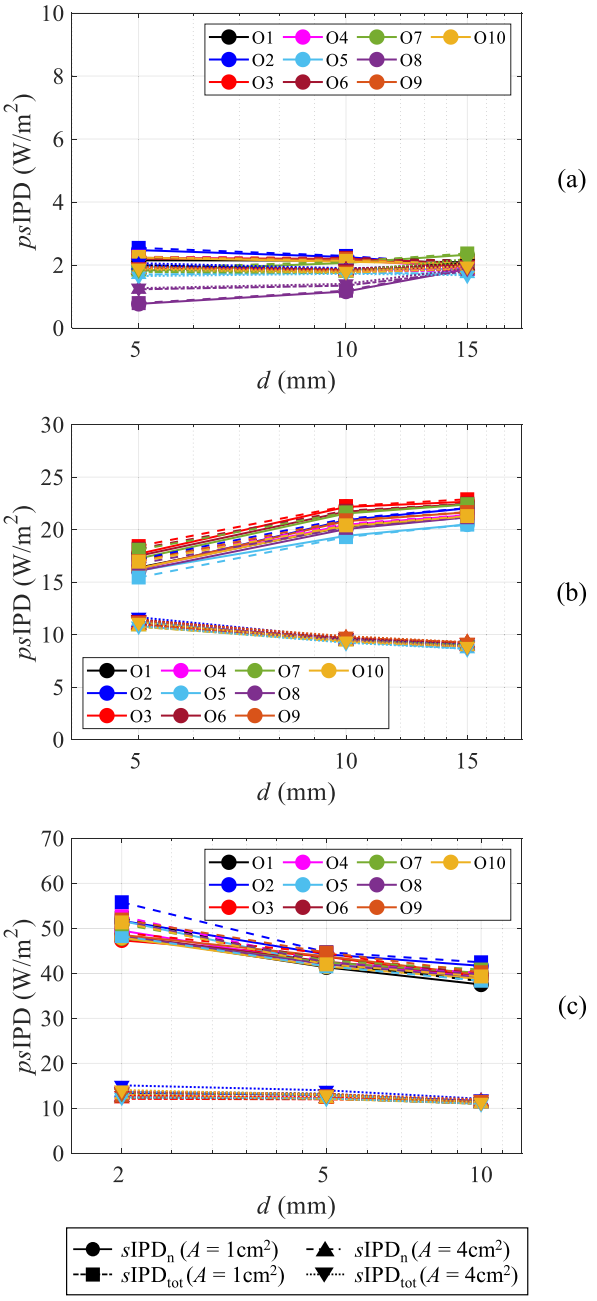

FIGURE 3. Spatially averaged incident power densities as a function of the antenna-to-skin separation distance for 4 × 4 dipole array at frequencies of (a) 10, (b) 30, and (c) 90 GHz.

In the case of the dipole antenna (Fig. 2), both $psIPD_n$ and $psIPD_{tot}$ decrease monotonically with an increase in the separation distance d. $psIPD_{tot}$ is greater than $psIPD_n$ in the 5–10 mm range at 10–30 GHz and the 2–5 mm range at 90 GHz. At $d > 10$ mm, all the results do not show any significant differences between the two definitions of the $sIPD$. The maximum absolute differences of the $psIPD$ among all the research groups are within 0.62, 0.45, and 0.43 dB respectively, at 10, 30, and 90 GHz when $d > 5$ mm.

For the 4 × 4 dipole array (Fig. 3), the profiles of both $psIPD_n$ and $psIPD_{tot}$ exhibit different trends compared to those of the dipole antennas owing to the dispersion of multiple near-field peaks generated by the wave source of the antenna array. Moreover, the difference between the $psIPD_n$ and $psIPD_{tot}$ was reduced.

The maximum absolute differences of $psIPD$ among all the organizations for the 4 × 4 dipole array are within 5.09, 0.77, and 0.6 dB respectively, at 10, 30, and 90 GHz when d is greater than 5 mm. The above results indicate that,

TABLE 6. Mean value and standard deviation of spatially averaged incident power densities for dipole antennas.

Distance (mm)	Frequency (GHz)	$psIPD_n$ (A=1cm^2)	$psIPD_{tot}$ (A=1cm^2)	$psIPD_n$ (A=4cm^2)	$psIPD_{tot}$ (A=4cm^2)
5	10	18.04 ± 0.65	20.62 ± 0.83	8.23 ± 0.16	11.28 ± 0.29
10		8.26 ± 0.26	8.72 ± 0.29	5.19 ± 0.12	6.09 ± 0.15
15		4.53 ± 0.1	4.66 ± 0.11	3.37 ± 0.06	3.7 ± 0.08
5	30	21.31 ± 0.33	25.34 ± 0.49	8.46 ± 0.1	12.09 ± 0.22
10		9.36 ± 0.15	9.99 ± 0.16	5.43 ± 0.06	6.51 ± 0.09
15		4.91 ± 0.13	5.08 ± 0.13	3.52 ± 0.05	3.91 ± 0.05
2	90	36.99 ± 0.9	56.53 ± 1.67	10.83 ± 0.39	20. 38 ± 0.99
5		21.92 ± 0.48	26.3 ± 0.62	8.55 ± 0.21	12.31 ± 0.33
10		9.55 ± 0.22	10.23 ± 0.24	5.49 ± 0.12	6.62 ± 0.15

Unit: W/m^2.

TABLE 7. Mean values and standard deviations of spatially averaged incident power densities for dipole antenna arrays.

Distance (mm)	Frequency (GHz)	$psIPD_n$ (A=1cm^2)	$psIPD_{tot}$ (A=1cm^2)	$psIPD_n$ (A=4cm^2)	$psIPD_{tot}$ (A=4cm^2)
5	10	2.02 ± 0.48	2.06 ± 0. 49	1.79 ± 0.21	1.84 ± 0.23
10		2.03 ± 0.32	2.06 ± 0.33	1.75 ± 0.15	1.79 ± 0.15
15		2.01 ± 0.13	2.05 ± 0.15	1.9 ± 0.1	1.96 ± 0.13
5	30	16.6 ± 0.62	17.21 ± 0.86	10.93 ± 0.16	11.3 ± 0.22
10		21.77 ± 0.84	20.85 ± 0.87	9.47 ± 0.14	9.56 ± 0.18
15		21.67 ± 0.69	21.72 ± 0.73	8.99 ± 0.19	9.0 ± 0.2
2	90	48.93 ± 1.55	51.95 ± 2.05	12.69 ± 0.51	13.59 ± 0.72
5		42.55 ± 1.0	43.03 ± 1.16	12.35 ± 0.37	13.0 ± 0.47
10		39.34 ± 1.07	39.85 ± 1.23	11.25 ± 0.22	11.57 ± 0.33

Unit: W/m^2.

at a separation distance $d > 5$ mm, there is no obvious discrepancy between the different EM-simulation and spatial average methods for the calculation of $psIPD_n$ and $psIPD_{tot}$ for either the dipole or dipole antenna arrays.

Tables 6 and 7 summarize the mean value and standard deviation of computed $psIPD_n$ and $psIPD_{tot}$ for the dipole and dipole array, respectively. The separation distances from the antenna for the cases of $d = 5$, 10, and 15 mm for 10–30 GHz and $d = 2$, 5, and 10 mm for 90 GHz were compared. The relative standard deviation (RSD), which is defined as the ratio of the standard deviation to the mean value, was analyzed as a metric for the intercomparison of different research groups.

For the dipole source, as presented in Table 6, the maximum RSD values of $psIPD$ were 4.05% ($d = 5$ mm), 2.58% ($d = 15$ mm), and 4.84% ($d = 2$ mm), respectively, at a frequency of 10–90 GHz. Conversely, for the case of the 4 × 4 dipole array, as presented in Table 7, the maximum RSD was approximately 23.55% ($d = 5$ mm), 5.0% ($d = 5$ mm), and 5.26% ($d = 2$ mm) at a frequency of 10–90 GHz. The above results agree well with the outcomes of previous WG activities (see Tables 6 and 7 in [41]). This shows that the impact on the calculation of the antenna near-field distribution in free space caused by the different numerical methods used by each organization is very small, demonstrating the effectiveness of EM-simulation methods for the antennas themselves.

B. COMPARISON OF PEAK SPATIAL-AVERAGE EPITHELIAL/ABSORBED POWER DENSITY

Figures 4 and 5 show the intercomparison results of the $psAPD$ as a function of the antenna-to-skin separation distance d exposed to the dipole when the averaging area A is 1 and 4 cm^2, respectively. In Figs. 4 and 5, the solid lines with circular markers indicate the results obtained using the one-layer model, whereas the dashed lines with square markers denote those obtained using the three-layer model.

As shown in Figs. 4 and 5, for both the one- and three-layer skin models exposed to a dipole antenna, the profiles of $psAPD$ decrease gradually as d increases. At 10 GHz, relatively large deviations are observed in the different organizations. The maximum absolute differences of $psAPD$ are 3.24 and 3.0 dB at $d = 5$ mm, respectively, for the one- and three-layer models when $A = 1$ cm^2. When A increases to 4 cm^2, the corresponding differences are reduced to 3.62 and 2.89 dB, respectively.

However, at frequencies ranging from 30–90 GHz, the deviations caused by the EM simulation methods are very small for both the one- and three-layer models. As shown in Figs. 4 (b) and (c) and Figs. 5 (b) and (c), the maximum absolute differences of $psAPD$ are within 1.07 and 2.46 dB, respectively, at 30 and 90 GHz when $A = 1$ cm^2. This difference is further reduced to 1.21 and 2.49 dB, respectively, for $A = 4$ cm^2.

Figures 6 and 7 show the intercomparison results of the $psAPD$ as a function of the antenna-to-skin separation distance d exposed to the radiation sources of the 4 × 4 dipole array when the average area A is 1 and 4 cm^2, respectively. Unlike the dipoles illustrated in Figs. 4 and 5, the deviation of $psAPDs$ at 10 GHz is nonexistent at $d = 5$ mm, but at $d = 15$ mm. The maximum absolute differences of $psAPD$ at 10 GHz are 9.84 and 10.15 dB at $d = 15$ mm when A is 1 and 4 cm^2, respectively.

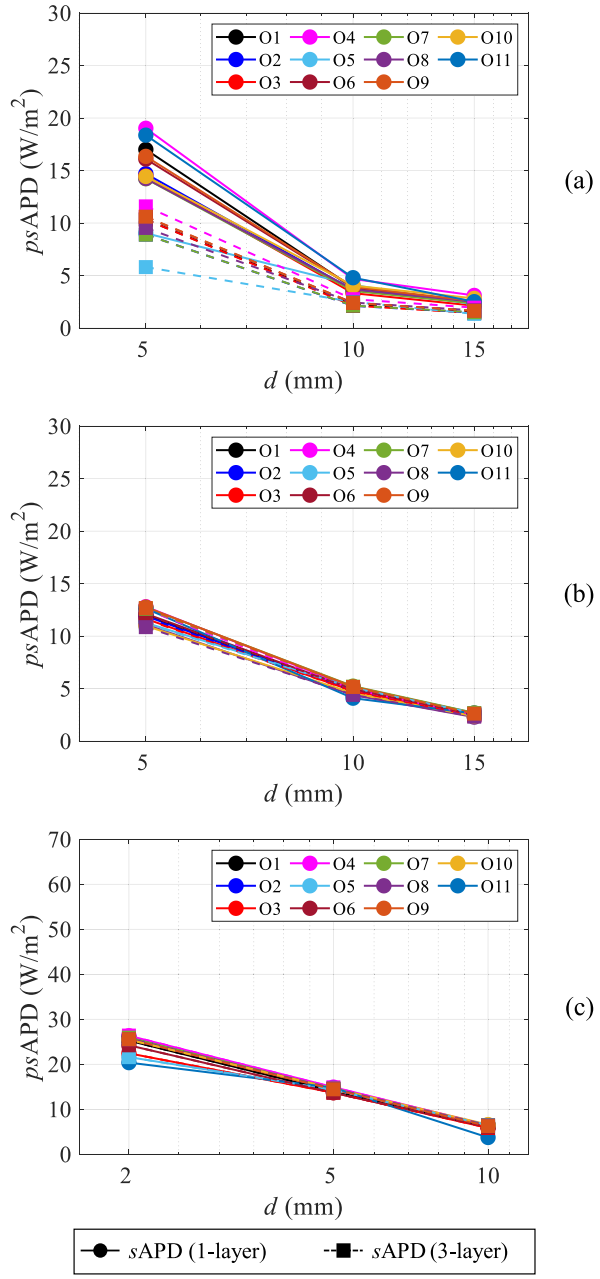

FIGURE 4. Spatially averaged epithelial/absorbed power density as a function of the antenna-to-skin separation distance for a dipole when A = 1 cm^2 at frequencies of (a) 10, (b) 30, and (c) 90 GHz.

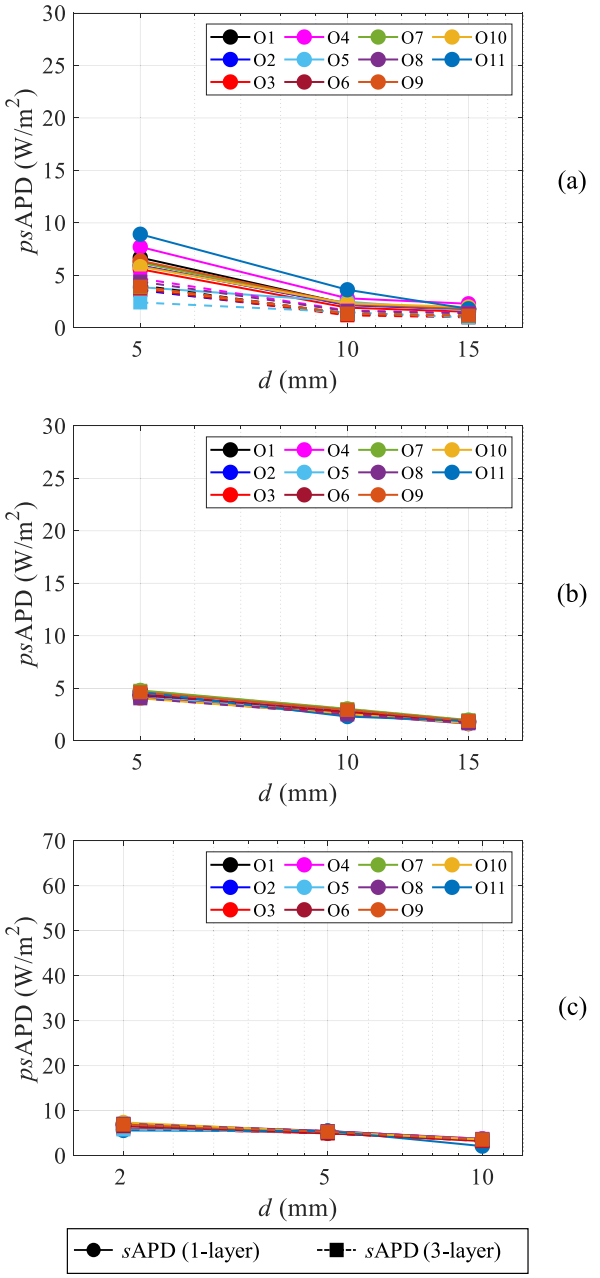

FIGURE 5. Spatially averaged epithelial/absorbed power density as a function of the antenna-to-skin separation distance for a dipole when A = 4 cm^2 at frequencies of (a) 10, (b) 30, and (c) 90 GHz.

Particularly at 30 GHz, there are also significant variations in the numerical results from the different research groups. The maximum absolute differences of the *ps*APD at 30 GHz increase to 5.49 and 4.27 dB at $d = 5$ mm when A is 1 and 4 cm^2, respectively. At 90 GHz, the largest deviation of *ps*APD changes at $d = 5$ mm to 2.75 and 2.74 dB, respectively, when A is 1 and 4 cm^2. Furthermore, similar to the results of the dipoles in Figs. 4 and 5, the difference in the *ps*APD values obtained using the one- and three-layer skin models is still small for the dipole arrays.

Tables 8 and 9 list the statistical mean values and standard deviations of *ps*APD for cases of the dipole and dipole array, respectively. For the dipole source (Table 8), the maximum RSD of the one-layer models were 20.0%, 8.03%, and 13.33%, which occurred at frequencies of 10 GHz when $d =$ 5 mm, 30 GHz when $d = 10$ mm, and 90 GHz when $d =$ 10 mm.

When using the three-layer skin models, the corresponding maximum RSD were 17.39%, 5.77%, and 7.02%, which occurred at 10 GHz when $d = 5$ mm, 30 GHz when $d =$ 5 mm, and 90 GHz when $d = 2$ mm.

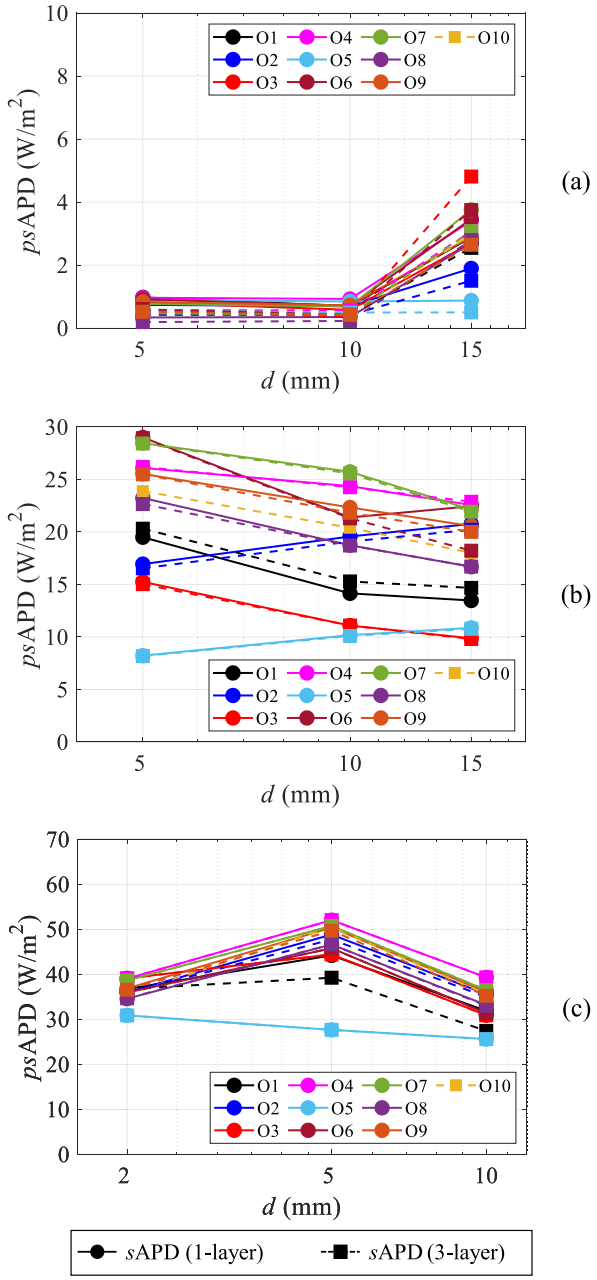

FIGURE 6. Spatially averaged epithelial/absorbed power density as a function of the antenna-to-skin separation distance for 4 × 4 dipole arrays when A = 1 cm^2 at frequencies of (a) 10, (b) 30, and (c) 90 GHz.

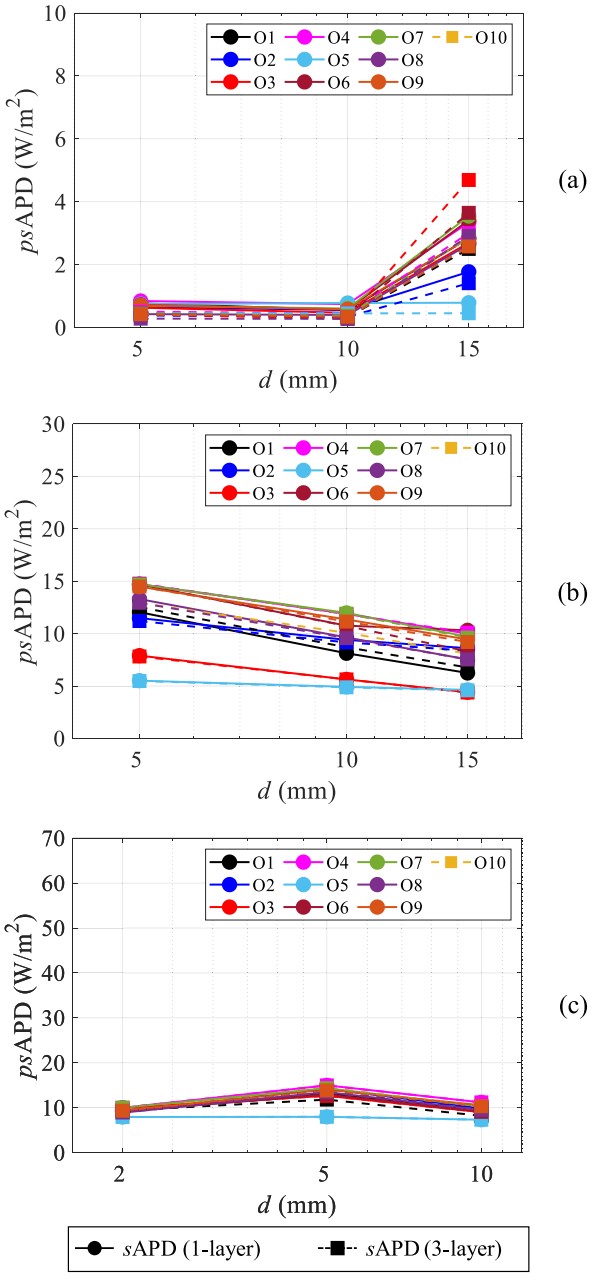

FIGURE 7. Spatially averaged epithelial/absorbed power density as a function of the antenna-to-skin separation distance for 4 × 4 dipole arrays when A = 4 cm^2 at frequencies of (a) 10, (b) 30, and (c) 90 GHz.

For the dipole array, as presented in Table 9, the maximum RSD of the one-layer models were 33.13%, 32.49%, and 12.07% at 10 GHz when $d = 15$ mm, 30 GHz when $d = 5$ mm, and 90 GHz when $d = 10$ mm, respectively. When using the three-layer skin models, the corresponding maximum RSDs were within 42.55%, 29.55%, and 16.7%, respectively, at 10 GHz when $d = 15$ mm, 30 GHz when $d = 5$ mm, and 90 GHz when $d = 5$ mm.

The above results indicate no evident difference exists between the *ps*APD values in the different organizations when using dipole antennas at 30 GHz and 90 GHz; however, some deviations occur at 10 GHz when $d = 5$ mm. The difference in the *ps*APD from 11 organizations when using the 4 × 4 dipole array was relatively greater than that of the dipole at 30 and 90 GHz. Additionally, a significant difference is observed at 10 GHz when $d = 15$ mm.

These facts indicate that a difference in the numerical analysis of the spatial-average APD among various organizations may exist depending on the different antenna types at specific frequency ranges as well as antenna-to-skin separation distances, whereas the difference caused by the skin models is relatively marginal. Particularly, when using a dipole

TABLE 8. Mean values and standard deviations of spatially averaged epithelial/absorbed power densities for dipole antennas.

Distance (mm)	Frequency (GHz)	One-layer		Three-layer	
		*ps*APD (A=1cm^2)	*ps*APD (A=4cm^2)	*ps*APD (A=1cm^2)	*ps*APD (A=4cm^2)
5	10	15.27 ± 2.67	6.31 ± 1.26	9.62 ± 1.67	3.85 ± 0.64
10		3.95 ± 0.45	2.42 ± 0.46	2.34 ± 0.21	1.4 ± 0.15
15		2.51 ± 0.27	1.83 ± 0.19	1.57 ± 0.18	1.16 ± 0.15
5	30	12.0 ± 0.68	4.39 ± 0.26	11.93 ± 0.64	4.38 ± 0.25
10		4.84 ± 0.36	2.74 ± 0.22	4.91 ± 0.24	2.79 ± 0.15
15		2.53 ± 0.13	1.8 ± 0.11	2.53 ± 0.11	1.81 ± 0.09
2	90	24.44 ± 2.04	6.67 ± 0.59	24.76 ± 1.68	6.71 ± 0.47
5		14.39 ± 0.43	5.27 ± 0.18	14.29 ± 0.43	5.24 ± 0.18
10		6.06 ± 0.8	3.42 ± 0.46	6.25 ± 0.22	3.54 ± 0.16

Unit: W/m^2.

TABLE 9. Mean values and standard deviations of spatially averaged epithelial/absorbed power densities for dipole antenna arrays.

Distance (mm)	Frequency (GHz)	One-layer		Three-layer	
		*ps*APD (A=1cm^2)	*ps*APD (A=4cm^2)	*ps*APD (A=1cm^2)	*ps*APD (A=4cm^2)
5	10	0.81 ± 0.19	0.69 ± 0.12	0.5 ± 0.12	0.42 ± 0.06
10		0.69 ± 0.16	0.58 ± 0.12	0.42 ± 0.09	0.35 ± 0.06
15		2.73 ± 0.88	2.65 ± 0.88	2.77 ± 1.16	2.69 ± 1.15
5	30	21.35 ± 6.94	12.09 ± 3.33	22.41 ± 6.62	12.65 ± 2.96
10		18.61 ± 5.63	9.3 ± 2.61	19.4 ± 4.69	9.7 ± 2.16
15		17.7 ± 5.13	7.87 ± 2.29	18.0 ± 3.8	7.98 ± 1.68
2	90	36.41 ± 2.59	9.33 ± 0.66	36.37 ± 2.58	9.33 ± 0.65
5		45.62 ± 7.31	13.08 ± 2.05	44.87 ± 7.5	12.87 ± 2.06
10		33.36 ± 4.03	9.6 ± 1.1	32.698 ± 4.37	9.4 ± 1.17

Unit: W/m^2.

array at 30 GHz, relatively large deviations were observed, regardless of the skin models. To determine the skewness and tail weights of the data batches, statistical analysis of

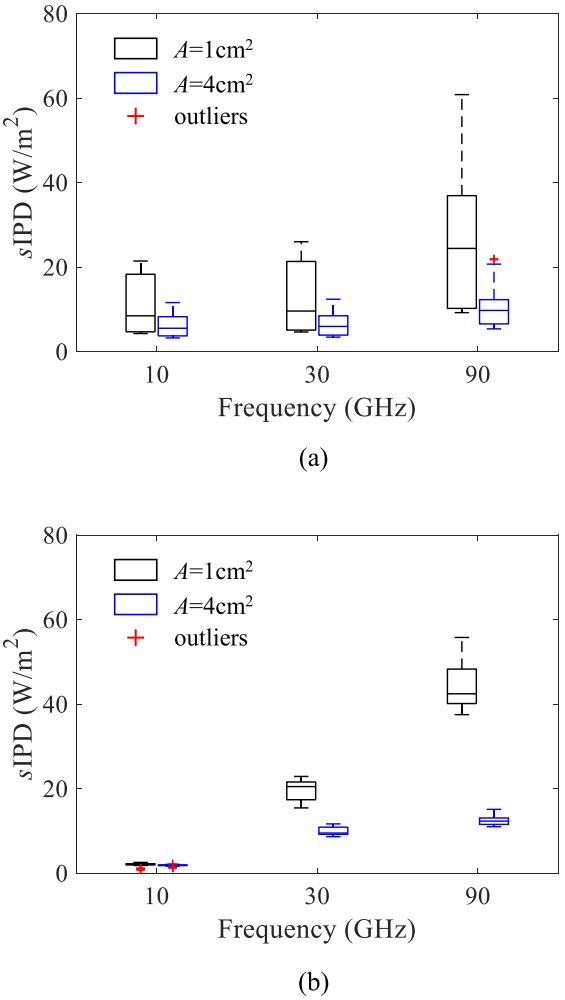

FIGURE 8. Statistical analysis of sIPD as a function of frequency from 10 to 90 GHz considering all the potential effects caused by the EM-method, antenna-to-skin separation distance, definition of power density, and averaging area: (a) single dipole and (b) 4 × 4 dipole arrays.

the significant differences in the calculated *s*PDs is conducted hereafter.

C. STATISTICAL ANALYSIS OF THE SIGNIFICANT DIFFERENCE

The variations in the *ps*APD values between the different groups in the previous sections suggest that they may be affected by the antennas types. In this section, the variability in *ps*APD caused by antenna models is evaluated.

Figures 8 and 9 show the box plots of the calculated *ps*IPD and *ps*APD, respectively, as a function of the frequency from 10 to 90 GHz. The results are shown in Figs. 8 (a-b) and 9(a-b), respectively, when using a half-wavelength dipole and 4 × 4 dipole array. In Figs. 8 and 9, the height of the rectangular box indicates the interquartile range (IQR), which is the range between the 75th and 25th percentiles. The horizontal line in the middle of the box denotes the statistical median value of *ps*PD from different groups. The error bars show the range of maximum to minimum values, where the

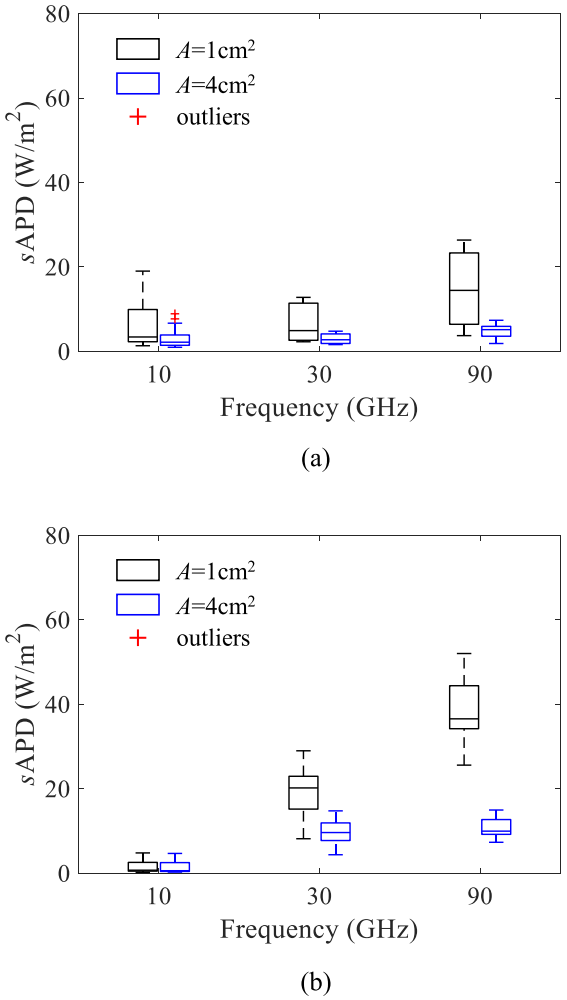

FIGURE 9. Statistical analysis of sAPD as a function of frequency from 10 to 90 GHz considering all the potential effects caused by the EM-method, antenna-to-skin separation distance, definition of power density, and averaging area: (a) single dipole and (b) 4 × 4 dipole arrays.

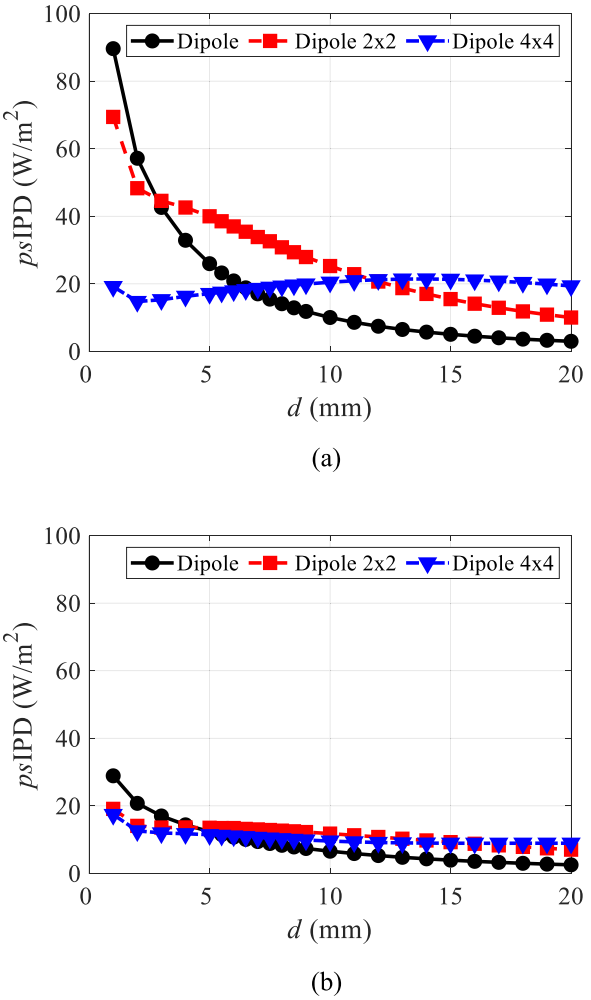

FIGURE 10. $sIPD_{tot}$ as a function of the antenna-to-skin separation distance with different antenna types of the single dipole, 2 × 2, and 4 × 4 dipole arrays at 30 GHz averaged over (a) 1 cm^2 and (b) 4 cm^2.

plus sign indicates the outliers. Notably, for each box with error bars, three sets of antenna-to-skin separation distances (5, 10, and 15 mm or 2, 5, and 10 mm) and two types of skin models (one- and three-layer; or two definitions for *s*IPD, namely, $sIPD_n$ and $sIPD_{tot}$) were included. Therefore, the 11 research groups provided a maximum of 66 sets of data in each frequency band and averaging area, which was sufficient for statistical analysis.

In Fig. 8 (a), for the *s*IPD values obtained using a dipole antenna, only one outlier was observed at 90 GHz when $A = 4\ cm^2$. When using a dipole array, as can be seen in Fig. 8 (b), four outliers appear at 10 GHz. However, the IQRs of the *s*IPD values for the dipole array cases are much smaller than those of the dipole antennas. For the *ps*APD values obtained using the dipole antennas, as illustrated in Fig. 9 (a), two outliers occurred at 10 GHz when $A = 4\ cm^2$. When the dipole array was used, there were no outliers. Conversely, the IQRs of the *ps*APD values for the dipole arrays at 30 and 90 GHz are comparable or even larger than those of the dipole antennas, particularly when $A = 1\ cm^2$. However, the deviation caused by the numerical calculation error is not evident for both the *ps*IPD and *ps*APD values.

D. VARIABILITY OF APD FOR THE DIPOLE ARRAY AT 30 GHz

As shown in Figs. 6 (b) and 7 (b), relatively large variations in the *ps*APD values occurred when using the 4 × 4 dipole array antennas at 30 GHz. In this section, the variability in the *ps*APD caused by the number of dipole antenna elements is evaluated.

Figures 10 and 11 show the calculated *ps*IPD and *ps*APD values, respectively, as a function of the antenna-to-skin separation distance d at 30 GHz, which were provided by O1. For simplicity, only the results for $sIPD_{tot}$ are shown in Fig. 10. Figs. 10 (a-b) and 11 (a-b) denote the average areas of 1 and 4 cm^2, respectively. To evaluate the impact of the number of antenna arrays, three different antenna types—half-wavelength single dipole, 2 × 2, and 4 × 4 dipole arrays—were compared.

As shown in Fig. 10 (a), all the results of *ps*IPD smoothly change with an increase in the antenna-to-skin separation d.

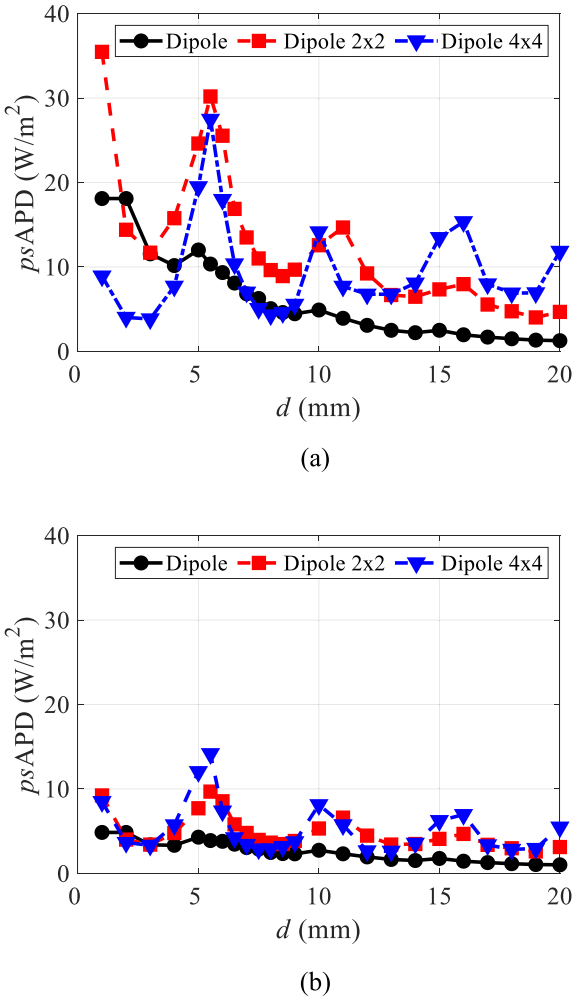

FIGURE 11. sAPD as a function of antenna-to-skin separation distance with different antenna types of single dipole, 2 × 2, and 4 × 4 dipole arrays at 30 GHz averaged over (a) 1 cm^2 and (b) 4 cm^2.

For the single dipole and 2 × 2 dipole arrays, the trends are close to monotonically decreasing as d increases. For the case of the 4 × 4 dipole array, the curve first exhibits an upward trend and then slowly declines as d increases. This may be due to the increased number of antenna arrays or dimensions, which changes the boundary conditions of the near field. However, when $A = 4$ cm^2, the above changes become less observable, as illustrated in Fig. 10 (b).

However, in Fig. 11 (a), the curves of *ps*APD when using the dipole arrays show evident periodic fluctuations as d increases. Particularly, at integer multiples of half wavelength, that is, 10 mm at 30 GHz, some bursts can be observed. This phenomenon did not change as the average area increased from 1 to 4 cm^2, as shown in Fig. 11 (b).

From the above results, it is deduced that, unlike the results of *ps*APD when using a single dipole, an increase in the number of dipole arrays may significantly change the mutual interaction between the antennas and skin models. This eventually results in a calculation error of *ps*APD at 5, 10, or 15 mm at 30 GHz, which corresponds well with the relatively large deviation shown in Figs. 6 (b) and 7 (b).

TABLE 10. Maximum absolute difference in spatially averaged epithelial/absorbed power densities due to different definitions using dipoles and dipole arrays investigated using FDTD method.

Distance (mm)	Frequency (GHz)	One-layer		Three-layer	
		ΔpsAPD (A=1cm^2)	ΔpsAPD (A=4cm^2)	ΔpsAPD (A=1cm^2)	ΔpsAPD (A=4cm^2)
Dipole	10	0.13 dB	0.04 dB	0.51 dB	0.26 dB
	30	0.13 dB	0.16 dB	0.11 dB	0.16 dB
	90	0.19 dB	0.2 dB	0.19 dB	0.2 dB
Dipole Array	10	0.12 dB	0.11 dB	0.41 dB	0.23 dB
	30	0.18 dB	0.18 dB	0.17 dB	0.17 dB
	90	0.19 dB	0.2 dB	0.19 dB	0.2 dB

TABLE 11. Maximum absolute difference in spatially averaged epithelial/absorbed power densities due to different definitions using dipoles and dipole arrays investigated using FEM method.

Distance (mm)	Frequency (GHz)	One-layer		Three-layer	
		ΔpsAPD (A=1cm^2)	ΔpsAPD (A=4cm^2)	ΔpsAPD (A=1cm^2)	ΔpsAPD (A=4cm^2)
Dipole	10	0.46 dB	0.42 dB	0.09 dB	0.69 dB
	30	0.49 dB	0.46 dB	0.46 dB	0.43 dB
	90	0.13 dB	0.12 dB	0.18 dB	0.17 dB
Dipole Array	10	0.15 dB	0.25 dB	1.3 dB	0.91 dB
	30	0.51 dB	0.5 dB	0.46 dB	0.46 dB
	90	0.23 dB	0.22 dB	0.22 dB	0.21 dB

E. VARIABILITY OF APD DEFINITION

In this intercomparison study, the formula for deriving the *s*APD was not unified among all research groups. Therefore, it is necessary to discuss the difference in the calculated *s*APD caused by the two definitions in (1) and (2), that is, the volumetric integral for the entire skin model and surface integral of the normal component of the Poynting vector perpendicular to the skin model, respectively, as recommended by the ICNIRP exposure guidelines [6].

Tables 10 and 11 list the results of the maximum absolute difference in *ps*APD (ΔpsAPD) due to different definitions using dipole and dipole array antennas evaluated by O6 and O8, which employed the numerical methods of the FDTD and FEM, respectively. The same separation-distance conditions and skin models were used.

In Table 10, for the FDTD method, the maximum ΔpsAPD caused by the use of different equations are within 0.2 dB for the dipole and dipole array at frequencies within 10−90 GHz when one-layer skin models are employed. When using the three-layer models, the corresponding difference did not exceed 0.51 dB. When using the FEM method, as shown in Table 11, the maximum ΔpsAPD slightly increases to within 0.49 and 0.51 dB, respectively, for cases of the dipole and dipole array at 10−90 GHz when the one-layer skin models are used. The corresponding difference is up to 0.69 and 1.3 dB, respectively, when using the three-layer skin models.

IV. DISCUSSION AND CONCLUSION

Compared with the intercomparison study of previous WG [40], [41], this study unified simulation conditions to the extent possible, such as the antenna type for the radiation source, planar skin model, and dielectric constants of body tissues, to minimize the number of variables that may affect the fairness of the intercomparison results. Moreover, the number of research groups as well as the EM-simulation algorithm have increased from the last 6 to 11. We believe that the established exposure scenarios considered in this study are more accurate and rigorous for clarifying the validity of the APD averaging method, which will be very informative for the next intercomparison of dosimetry analysis using more realistic body models.

In the first step of the intercomparison of the peak value of spatially averaged incident power densities, that is, $ps\text{IPD}_\text{n}$ and $ps\text{IPD}_\text{tot}$, all the results provided by the eleven groups showed good agreement with each other. For the cases using dipole antennas, the maximum RSDs among the different organizations were 4.04%, 2.58%, and 4.84% at frequencies of 10, 30, and 90 GHz, respectively. For the dipole array, the maximum RSDs did not exceed 23.55%, 5.0%, and 5.26% at frequencies of 10, 30, and 90 GHz, respectively. Relatively large deviations of up to 23.55% were observed for the dipole arrays at 10 GHz when $d = 5$ mm. For a large dimension of an array with 16 dipole elements, this distance can be regarded as an extreme near-field at 10 GHz. In this case, it is understandable that the difference in the electromagnetic field distribution obtained by different simulation methods increases owing to different approaches for solving Maxwell equations with different boundary conditions and resolutions. Additionally, the maximum RSDs of all the results did not exceed 5.26%. The above results are in agreement with the outcomes from a previous study (Tables 6 and 7 in [41]), demonstrating the effectiveness of all the employed methods for the EM simulation of the antenna near-field distribution.

As the second step of intercomparison for the peak value of spatially averaged epithelial/absorbed power densities, that is, psAPD, an excellent agreement for the considered exposure scenarios using a dipole antenna can still be observed. At frequencies of 10, 30, and 90 GHz, the maximum RSDs among different organizations were 18.83%, 8.03%, and 13.33%, respectively, for both the one- and three-layer skin models. When using dipole arrays as the radiation source, relatively obvious deviations in the calculated psAPD are shown in several scenarios (e.g., 10 GHz at $d = 15$ mm, 30 GHz when d is from 5 to 15 mm, and 90 GHz at $d = 10$ mm). Despite this, the maximum RSDs for the cases using the dipole arrays did not exceed 42.55%, 29.55%, and 16.7%, respectively, at frequencies of 10, 30, and 90 GHz, regardless of the skin model. Based on the statistical significance analysis, the number of outliers is very small compared to the overall sample of the calculated data, including all the parameters of the antenna types, skin models, and separation distance. Furthermore, it is confirmed that the maximum difference caused by the equations of deriving the sAPD recommended by the ICNIRP exposure guidelines, i.e., the volumetric integral for the entire skin model and surface integral of the normal component of the Poynting vector perpendicular to the skin model, is generally approximately 0.5 to 1 dB or even less. The difference depends on the calculation condition, e.g., field segmentation; here, we found that the difference can be suppressed to approximately 0.2 dB or lower in almost all exposure scenarios.

This study represents the first intercomparison of the calculated sAPD in a simplified body model for exposure from different antennas ranging from 10 GHz to 90 GHz. The main causes of variance in the numerical calculations in the dosimetry analysis of psAPD were evaluated using an objective comparison of the analysis results from different research groups. The fair agreement among the intercomparison results demonstrated that deviations caused by the numerical method, definition, and spatial average of the calculated psAPD using planar skin models are marginal. However, with the increasing number of antenna arrays, the dependence on the antenna types that are used as the radiation sources for the dosimetry analysis of sAPD may be slightly increased.

REFERENCES

[1] A. Hirata, Y. Diao, T. Onishi, K. Sasaki, S. Ahn, D. Colombi, V. De Santis, I. Laakso, L. Giaccone, W. Joseph, E. A. Rashed, W. Kainz, and J. Chen, "Assessment of human exposure to electromagnetic fields: Review and future directions," *IEEE Trans. Electromagn. Compat.*, vol. 63, no. 5, pp. 1619–1630, Oct. 2021.

[2] W. H. Bailey, R. Bodemann, J. Bushberg, C.-K. Chou, R. Cleveland, and A. Faraone, "Synopsis of IEEE Std C95. 1Ů-2019 'IEEE standard for safety levels with respect to human exposure to electric, magnetic, and electromagnetic fields, 0 Hz to 300 GHz,'" *IEEE Access*, vol. 7, pp. 171346–171356, 2019.

[3] M. Zhadobov, N. Chahat, R. Sauleau, C. Le Quement, and Y. Le Drean, "Millimeter-wave interactions with the human body: State of knowledge and recent advances," *Int. J. Microw. Wireless Technol.*, vol. 3, no. 2, pp. 237–247, 2011.

[4] T. Wu, R. Peng, L. Zhang, and K. Li, "Editorial: Human exposure to new-emerging electric, magnetic and electromagnetic fields," *Frontiers Public Health*, vol. 10, Apr. 2022, Art. no. 894624.

[5] *IEEE Standard for Safety Levels with Respect to Human Exposure to Electric, Magnetic and Electromagnetic Fields, 0 Hz to 300 GHz*, New York, NY, USA, Standard IEEE-C95.1, 2019.

[6] International Commission on Non-Ionizing Radiation Protection, "Guidelines for limiting exposure to electromagnetic fields (100 kHz to 300 GHz)," *Health Phys.*, vol. 118, no. 5, pp. 483–524, May 2020.

[7] K. Foster and D. Colombi, "Thermal response of tissue to RF exposure from canonical dipoles at frequencies for future mobile communication systems," *Electron. Lett.*, vol. 53, no. 5, pp. 360–362, Mar. 2017.

[8] K. R. Foster, M. C. Ziskin, and Q. Balzano, "Thermal modeling for the next generation of radiofrequency exposure limits: Commentary," *Health Phys.*, vol. 113, no. 1, pp. 41–53, 2017.

[9] M. C. Ziskin, S. I. Alekseev, K. R. Foster, and Q. Balzano, "Tissue models for RF exposure evaluation at frequencies above 6 GHz," *Bioelectromagnetics*, vol. 39, no. 3, pp. 173–189, Apr. 2018.

[10] K. R. Foster, M. C. Ziskin, Q. Balzano, and A. Hirata, "Transient thermal responses of skin to pulsed millimeter waves," *IEEE Access*, vol. 8, pp. 130239–130251, 2020.

[11] K. R. Foster, M. C. Ziskin, and Q. Balzano, "Time-temperature thresholds and safety factors for thermal hazards from radiofrequency energy above 6 GHz," *Health Phys.*, vol. 121, no. 3, pp. 234–247, Sep. 2021.

[12] K. R. Foster, M. C. Ziskin, and Q. Balzano, "Thermal response of human skin to microwave energy: A critical review," *Health Phys.*, vol. 111, no. 6, pp. 528–541, Dec. 2016.

[13] S. I. Alekseev, A. A. Radzievsky, M. K. Logani, and M. C. Ziskin, "Millimeter wave dosimetry of human skin," *J. Bioelectromagnetics Soc.*, vol. 29, no. 1, pp. 65–70, Jan. 2008.

[14] A. Kanezaki, A. Hirata, S. Watanabe, and H. Shirai, "Effects of dielectric permittivities on skin heating due to millimeter wave exposure," *Biomed. Eng. OnLine*, vol. 8, no. 1, p. 20, Dec. 2009.

[15] A. Kanezaki, A. Hirata, S. Watanabe, and H. Shirai, "Parameter variation effects on temperature elevation in a steady-state, one-dimensional thermal model for millimeter wave exposure of one-and three-layer human tissue," *Phys. Med. Biol.*, vol. 55, no. 16, pp. 4647–4659, 2010.

[16] K. Sasaki, M. Mizuno, and K. Wake, "Monte Carlo simulations of skin exposure to electromagnetic field from 10 GHz to 1 THz," *Phys. Med. Biol.*, vol. 62, no. 17, pp. 6993–7010, 2017.

[17] K. Li, K. Sasaki, S. Watanabe, and H. Shirai, "Relationship between power density and surface temperature elevation for human skin exposure to electromagnetic waves with oblique incidence angle from 6 GHz to 1 THz," *Phys. Med. Biol.*, vol. 64, no. 6, Mar. 2019, Art. no. 065016.

[18] K. Li, "Multivariate regression analysis of skin temperature rises for millimeter-wave dosimetry," *IEEE Trans. Electromagn. Compat.*, vol. 64, no. 4, pp. 941–950, Aug. 2022.

[19] K. Li and K. Sasaki, "Monte Carlo simulation of clothed skin exposure to electromagnetic field with oblique incidence angles at 60 GHz," *Frontiers Public Health*, vol. 10, Feb. 2022, Art. no. 795414.

[20] A. Christ, T. Samaras, E. Neufeld, and N. Kuster, "RF-induced temperature increase in a stratified model of the skin for plane-wave exposure at 6–100 GHz," *Radiat. Protection Dosimetry*, vol. 188, no. 3, pp. 350–360, Jun. 2020.

[21] G. Sacco, S. Pisa, and M. Zhadobov, "Impact of textile on electromagnetic power and heating in near-surface tissues at 26 GHz and 60 GHz," *IEEE J. Electromagn., RF Microw. Med. Biol.*, vol. 5, no. 3, pp. 262–268, Sep. 2021.

[22] W. He, B. Xu, M. Gustafsson, Z. Ying, and S. He, "RF compliance study of temperature elevation in human head model around 28 GHz for 5G user equipment application: Simulation analysis," *IEEE Access*, vol. 6, pp. 830–838, 2018.

[23] K. Sasaki, K. Li, J. Chakarothai, T. Iyama, T. Onishi, and S. Watanabe, "Error analysis of a near-field reconstruction technique based on plane wave spectrum expansion for power density assessment above 6 GHz," *IEEE Access*, vol. 7, pp. 11591–11598, 2019.

[24] Y. Diao and A. Hirata, "Exposure assessment of array antennas at 28 GHz using hybrid spherical near-field transformation and FDTD method," *IEEE Trans. Electromagn. Compat.*, vol. 63, no. 5, pp. 1690–1698, Oct. 2021.

[25] S. Omi, K. Sasaki, and K. Wake, "Performance analysis of incident power density evaluation by inverse source method for compliance assessment at quasi-millimeter and millimeter wave bands," *IEEE Trans. Electromagn. Compat.*, vol. 63, no. 5, pp. 1649–1657, Oct. 2021.

[26] B. Xu, K. Zhao, Z. Ying, D. Sjöberg, W. He, and S. He, "Analysis of impacts of expected RF EMF exposure restrictions on peak EIRP of 5G user equipment at 28 GHz and 39 GHz bands," *IEEE Access*, vol. 7, pp. 20996–21005, 2019.

[27] D. Colombi, B. Thors, C. TöRnevik, and Q. Balzano, "RF energy absorption by biological tissues in close proximity to mmW 5G wireless equipment," *IEEE Access*, vol. 6, pp. 4974–4981, 2018.

[28] E. Carrasco, D. Colombi, K. R. Foster, M. Ziskin, and Q. Balzano, "Exposure assessment of portable wireless devices above 6 GHz," *Radiat. Prot. Dosim.*, vol. 183, no. 4, pp. 489–496, Jun. 2019.

[29] B. Thors, D. Colombi, Z. Ying, T. Bolin, and C. Törnevik, "Exposure to RF EMF from array antennas in 5G mobile communication equipment," *IEEE Access*, vol. 4, pp. 7469–7478, 2016.

[30] D. Funahashi, T. Ito, A. Hirata, T. Iyama, and T. Onishi, "Averaging area of incident power density for human exposure from patch antenna arrays," *IEICE Trans. Electron.*, vol. E101.C, no. 8, pp. 644–646, Aug. 2018.

[31] N. Miura, S. Kodera, Y. Diao, J. Higashiyama, Y. Suzuki, and A. Hirata, "Power absorption and skin temperature rise from simultaneous near-field exposure at 2 and 28 GHz," *IEEE Access*, vol. 9, pp. 152140–152149, 2021.

[32] A. Hirata, S. Kodera, K. Sasaki, J. Gomez-Tames, I. Laakso, A. Wood, S. Watanabe, and K. R. Foster, "Human exposure to radiofrequency energy above 6 GHz: Review of computational dosimetry studies," *Phys. Med. Biol.*, vol. 66, no. 8, Apr. 2021, Art. no. 08TR01.

[33] Y. Hashimoto, A. Hirata, R. Morimoto, S. Aonuma, I. Laakso, K. Jokela, and K. R. Foster, "On the averaging area for incident power density for human exposure limits at frequencies over 6 GHz," *Phys. Med. Biol.*, vol. 62, no. 8, pp. 3124–3138, Apr. 2017.

[34] T. Nakae, D. Funahashi, J. Higashiyama, T. Onishi, and A. Hirata, "Skin temperature elevation for incident power densities from dipole arrays at 28 GHz," *IEEE Access*, vol. 8, pp. 26863–26871, 2020.

[35] A. L. Kapetanović and D. Poljak, "Assessment of incident power density on spherical head model up to 100 GHz," *IEEE Trans. Electromagn. Compat.*, vol. 64, no. 5, pp. 1296–1303, Oct. 2022.

[36] A. Hirata, D. Funahashi, and S. Kodera, "Setting exposure guidelines and product safety standards for radio-frequency exposure at frequencies above 6 GHz: Brief review," *Ann. Telecommun.*, vol. 74, nos. 1–2, pp. 17–24, Feb. 2019.

[37] R. Morimoto and A. Hirata, "Assessment of incident power density in different shapes of averaging area for radio-frequency exposure above 6 GHz," *Phys. Med. Biol.*, vol. 67, no. 21, Oct. 2022, Art. no. 215014.

[38] Y. Diao and A. Hirata, "Assessment of mmWave exposure from antenna based on transformation of spherical wave expansion to plane wave expansion," *IEEE Access*, vol. 9, pp. 111608–111615, 2021.

[39] M. Ziane, M. Zhadobov, and R. Sauleau, "High-resolution technique for near-field power density measurement accounting for antenna/body coupling at millimeter waves," *IEEE Antennas Wireless Propag. Lett.*, vol. 20, no. 11, pp. 2151–2155, Nov. 2021.

[40] *IEEE Guide for the Definition of Incident Power Density to Correlate Surface Temperature Elevation*, Standard IEEE Std 2889TM, Dec. 2021.

[41] K. Li, Y. Diao, K. Sasaki, A. Prokop, D. Poljak, V. Doric, J. Xi, S. Kodera, A. Hirata, and W. E. Hajj, "Intercomparison of calculated incident power density and temperature rise for exposure from different antennas at 10–90 GHz," *IEEE Access*, vol. 9, pp. 151654–151666, 2021.

[42] Y. Diao, K. Li, K. Sasaki, S. Kodera, I. Laakso, W. E. Hajj, and A. Hirata, "Effect of incidence angle on the spatial-average of incident power density definition to correlate skin temperature rise for millimeter wave exposures," *IEEE Trans. Electromagn. Compat.*, vol. 63, no. 5, pp. 1709–1716, Oct. 2021.

[43] D. Funahashi, A. Hirata, S. Kodera, and K. R. Foster, "Area-averaged transmitted power density at skin surface as metric to estimate surface temperature elevation," *IEEE Access*, vol. 6, pp. 77665–77674, 2018.

[44] Y. Diao, E. A. Rashed, and A. Hirata, "Assessment of absorbed power density and temperature rise for nonplanar body model under electromagnetic exposure above 6 GHz," *Phys. Med. Biol.*, vol. 65, no. 22, Nov. 2020, Art. no. 224001.

[45] K. Li, K. Sasaki, K. Wake, T. Onishi, and S. Watanabe, "Quantitative comparison of power densities related to electromagnetic near-field exposures with safety guidelines from 6 to 100 GHz," *IEEE Access*, vol. 9, pp. 115801–115812, 2021.

[46] G. Sacco, Z. Haider, and M. Zhadobov, "Exposure levels induced in curved body parts at mmWaves," *IEEE J. Electromagn., RF Microw. Med. Biol.*, vol. 6, no. 3, pp. 413–419, Sep. 2022.

[47] K. Taguchi, S. Kodera, A. Hirata, and T. Kashiwa, "Computation of absorbed power densities in high-resolution head models by considering skin thickness in quasi-millimeter and millimeter wave bands," *IEEE J. Electromagn., RF Microw. Med. Biol.*, vol. 6, no. 4, pp. 516–523, Dec. 2022.

[48] B. B. Beard, W. Kainz, T. Onishi, T. Iyama, S. Watanabe, O. Fujiwara, J. Wang, G. Bit-Babik, J. Wiart, and A. Faraone, "Comparisons of computed mobile phone induced SAR in the SAM phantom to that in anatomically correct models of the human head," *IEEE Trans. Electromagn. Compat.*, vol. 48, no. 2, pp. 397–407, May 2006.

[49] S. Gabriel, R. W. Lau, and C. Gabriel, "The dielectric properties of biological tissues: III. Parametric models for the dielectric spectrum of tissues," *Phys. Med. Biol.*, vol. 41, no. 11, pp. 2271–2293, 1996.
[50] C. Gabriel, "Compilation of the dielectric properties of body tissues at RF and microwave frequencies," Occupational Environ. Health Directorate Radiofrequency Radiat. Division, Brooks Air Force Base, San Antonio, TX, USA, Tech. Rep. N.AL/OE-TR-1996-0037, 1996.
[51] P. A. Hasgall. (May 15, 2018). *IT'IS Database for Thermal and Electromagnetic Parameters of Biological Tissues*, version 4.0. [Online]. Available: http://www.itis.swiss/database
[52] A. Taflove and S. C. Hagness, *Computational Electrodynamics: The Finite-Difference Time-Domain Method*, 3rd ed. Norwood, MA, USA: Artech House, 2005.
[53] D. Poljak, *Advanced Modeling in Computational Electromagnetic Compatibility*, Hoboken, NJ, USA: Wiley, 2007.
[54] T. Weiland, "A discretization method for the solution of Maxwell's equations for six-component fields," *Archiv Elektronik Uebertragungstechnik*, vol. 31, pp. 116–120, Mar. 1977.
[55] T. Weiland, M. Timm, and I. Munteanu, "A practical guide to 3-D simulation," *IEEE Microw. Mag.*, vol. 9, no. 6, pp. 62–75, Dec. 2008.
[56] P. B. Johns, "A symmetrical condensed node for the TLM method," *IEEE Trans. Microw. Theory Techn.*, vol. MTT-35, no. 4, pp. 370–377, Apr. 1987.

KUN LI (Member, IEEE) received the B.E. degree in communication engineering from the Nanjing University of Posts and Telecommunications, Nanjing, China, in 2011, and the M.E. and Ph.D. degrees in electrical engineering from the University of Toyama, Toyama, Japan, in 2014 and 2017, respectively.

From 2017 to 2019, he was a Researcher with the Electromagnetic Compatibility Laboratory, National Institute of Information and Communications Technology, Tokyo, Japan. In 2020, he joined Kagawa University, Japan, where he is currently working as an Assistant Professor. He is also a Visiting Researcher with the CNRS/IETR, University of Rennes 1, Rennes, France. His research interests include safety assessment of radio frequency radiation exposure to the human body and bio-EMC issues in microwave, millimeter and THz bands, and antenna design and over-the-air testing for wireless body area network systems.

Dr. Li is a member of the IEEE International Committee on Electromagnetic Safety TC95. He is a Senior Member of URSI and a member of IEICE. He was a recipient of the Young Scientist Award of the URSI, in 2020, the Risaburo Sato Award of EMC Sapporo & AMPEC, in 2019, the IEEE AP-S Japan Student Award, in 2015, and the IEICE Best Letter Award, in 2017. He is the Co-Chair of Working Group under Subcommittee 6 EMF Dosimetry Modeling established to study average schemes and assessment methods of absorbed power density.

SACHIKO KODERA (Member, IEEE) received the B.E. and M.E. degrees in electrical and computer engineering and the Ph.D. degree in computer science from the Nagoya Institute of Technology, Nagoya, Japan, in 2002, 2006, and 2019, respectively.

In 2016, she joined the Department of Electrical and Mechanical Engineering, Nagoya Institute of Technology, where she is currently an Associate Professor. Her current research interests include electromagnetic and thermal dosimetry modeling in humans for radio frequency and ambient heat exposures.

Dr. Kodera is a member of the Subcommittee 6 in IEEE International Committee on Electromagnetic Safety (ICES) Technical Committee 95. She received the Prizes for Science and Technology (Public Understanding Promotion Category, in 2020) from the Commendation for Science and Technology, Minister of Education, Culture, Sports, Science, and Technology, Japan, and Japan Open Innovation Prize (President of the Science Council of Japan Prize, in 2022) from the Cabinet Office.

DRAGAN POLJAK (Senior Member, IEEE) received the Ph.D. degree in electrical engineering from the University of Split, Croatia, in 1996. He is currently a Full Professor with the Department of Electronics and Computing, University of Split. He is also involved in ITER Physics EUROfusion Collaboration and in the Croatian Center for Excellence in Research for Technology Sciences. He has published more than 160 journals and 250 conference papers, and authored some books, e.g. two by Wiley, Hoboken, NJ, USA, and one by Elsevier, St. Louis, MO, USA. His research interests include computational electromagnetics (electromagnetics compatibility, bioelectromagnetics, and plasma physics). From May 2013 to June 2021, he was a member of the Board of the Croatian Science Foundation. He is a member of Editorial Board of *Engineering Analysis with Boundary Elements*, *Mathematical Problems in Engineering*, and *IET Science, Measurement & Technology*. He was awarded by several prizes for his achievements, such as the National Prize for Science, in 2004, the Croatian Section of IEEE Annual Award, in 2016, the Technical Achievement Award of the IEEE EMC Society, in 2019, and the George Green Medal from University of Mississippi, in 2021. He is active in few working groups of IEEE/International Committee on Electromagnetic Safety (ICES) Technology Committee 95 SC6 EMF Dosimetry Modeling.

YINLIANG DIAO (Member, IEEE) received the B.E. degree in electronic information engineering from Chongqing University, Chongqing, China, in 2008, the M.S. degree in electronic engineering from the Beijing University of Posts and Telecommunications, Beijing, China, in 2011, and the Ph.D. degree in electronic engineering from the City University of Hong Kong, in 2016.

Since 2017, he has been an Assistant Professor with South China Agricultural University, Guangzhou, China. From 2019 to 2021, he worked as a Research Assistant and an Associate Professor with the Nagoya Institute of Technology, where he is currently a Guest Associate Professor. His current research interests include electromagnetic dosimetry modeling and electromagnetic compatibility.

Dr. Diao is a member of IEEE ICES Standards Coordinating Committee and a member of the Scientific Expert Group of International Commission on Non-Ionizing Radiation Protection. He was a recipient of the Young Scientist Award from URSI GASS 2020.

KENSUKE SASAKI (Member, IEEE) received the B.E., M.E., and Ph.D. degrees in electrical and electronic engineering from Tokyo Metropolitan University, Tokyo, Japan, in 2006, 2008, and 2011, respectively.

He is currently with the National Institute of Information and Communications Technology (NICT), Tokyo. His research interests include electromagnetic theory, bioelectromagnetics, and dielectric properties measurement.

Dr. Sasaki was a member of the Scientific Expert Group of International Commission on Non-Ionizing Radiation Protection (ICNIRP), from 2018 to 2020. He was a recipient of the 2009 Young Scientist Award of the URSI, the 2012 Best Paper Award of the IEEJ, and the 2020 Achievement Award of the IEICE. He has been the Early Carrier Representative of Commission K, the International Scientific Radio Union (URSI), since 2017.

ANNA ŠUŠNJARA (Member, IEEE) received the Ph.D. degree in electrical engineering from the University of Split, Croatia, in 2021.

From 2015 to 2021, she was involved in the ITER Physics EUROfusion collaboration. In 2021, she joined a work group within IFMIF-DONES Project. She is currently a Postdoctoral Researcher with the Department of Electronics and Computing, University of Split. She gave a seminars/lectures about numerical modeling in computational electromagnetic at several European academic institutions and tutorials at international scientific conferences. She has authored or coauthored 16 journals and more than 35 conference papers. Her research interests include numerical modeling, uncertainty quantification, and sensitivity analysis in computational electromagnetics, particularly in bioelectromagnetism.

Dr. Šušnjara is a member of EBEA Societies. She was awarded with National Prize for Science, in 2021. In 2016, she received the Best Poster Award at BioEM Conference and spent one month at the Politecnico di Torino as an ACRI Awardee in Young Investigator Training Program. She serves as a reviewer for seven journals and two conferences. She also serves as the Vice President of Croatian Chapter for IEEE EMC Society. A complete list of her publications can be found at: https://www.bib.irb.hr/pregled/znanstvenici/348056

ALEXANDER PROKOP (Senior Member, IEEE) received the M.S. degree in electrical engineering and the Ph.D. degree in computational electromagnetics from the Technische Universität Darmstadt, Darmstadt, Germany, in 1997 and 2004, respectively.

He joined the Research and Development Department of CST, in 1998. He is currently the Bioelectromagnetics Applications Director of the SIMULIA Research and Development, Dassault Systèmes. Since 2006, he has been participating in the development of several IEEE/IEC standards on simulation methods and human exposure assessment. He is also Convenor of IEC TC 106 and IEEE ICES TC34 Subcommittees and working groups on computational SAR assessment JMT 62704-3 for mobile phones and JMT 62704-4 using the finite element method. In IEEE APS/SC, he leads a working group within P2816 on simulation of antennas using the TLM method. His research interests include anatomical human body modeling and computational biomedical simulation workflows.

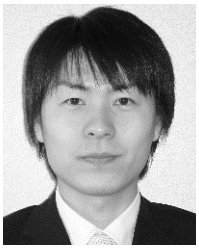

KENJI TAGUCHI (Member, IEEE) received the B.E., M.E., and Ph.D. degrees in electrical and electronic engineering from the Kitami Institute of Technology, Kitami, Japan, in 2001, 2003, and 2006, respectively.

From 2006 to 2009, he was an Assistant Professor with the Department of Information and Communication Engineering, Kumamoto National College of Technology. Since 2009, he has been an Associate Professor with the Department of Electrical and Electronic Engineering, Kitami Institute of Technology. His research interests include the analysis of electromagnetic fields, electromagnetic compatibility, and optimization problems. He is a Secretary of Task Force under EMF Dosimetry Modeling of IEEE International Committee on Electromagnetic Safety.

JINGTIAN XI (Member, IEEE) received the B.E. and M.E. degrees in electronic and information engineering from the South China University of Technology, Guangzhou, China, in 2003 and 2006, respectively, and the Ph.D. degree in microelectronics and solid-state electronics from Fudan University, Shanghai, China, in 2009. From 2009 to 2017, he was a Senior Researcher at the Logistics and Supply Chain MultiTech Research and Development Centre (LSCM) founded by the Government of the Hong Kong Special Administrative Region and affiliated to Hong Kong University. Since 2017, he has been a Project Leader with the Foundation for Research on Information Technologies in Society (IT'IS), Zurich, Switzerland. He has authored or coauthored more than 30 publications in journals and conferences, and held five patents. His current research interests include antenna design, RF dosimetry, and verification and validation (V&V) of numerical/measurement solutions for assessing exposure from electromagnetic sources. He has served as a technical program committee (TPC) member for multiple conferences and a reviewer for various IEEE journals.

SHUAI ZHANG (Senior Member, IEEE) received the B.E. degree from the University of Electronic Science and Technology of China, Chengdu, China, in 2007, and the Ph.D. degree in electromagnetic engineering from the Royal Institute of Technology (KTH), Stockholm, Sweden, in 2013. After his Ph.D. studies, he was a Postdoctoral Researcher at KTH. From 2010 to 2011, he was a Visiting Researcher at Lund University, Sweden, and Sony Mobile Communications AB, Sweden, respectively. In April 2014, he joined Aalborg University, Denmark, where he is currently working as an Associate Professor and the Head of the Antenna Research Group. He was also an External Antenna Specialist at Bang & Olufsen, Denmark, from 2016 to 2017. He has coauthored over 100 articles in well-reputed international journals and over 16 (U.S. or WO) patents. His current research interests include mmwave antennas for cellular communications, biological effects, metasurfaces, CubeSat antennas, massive MIMO antenna arrays, wireless sensors, and RFID antennas.

MING YAO (Graduate Student Member, IEEE) was born in 1994. He received the B.Eng. and M.Eng. degrees from the University of Electronic Science and Technology of China, Chengdu, China, in 2017 and 2020, respectively. He is currently pursuing the Ph.D. degree in wireless communication with the Antennas, Propagation, and Millimeter-Wave Systems Section, Department of Electronic Systems, Aalborg University, Aalborg, Denmark. His current research interests include antenna design, holographic metasurface, and EMF health and safety.

GIULIA SACCO (Member, IEEE) received the M.S. degree (summa cum laude) in biomedical engineering and the Ph.D. degree (cum laude and with the Doctor Europaeus label) in information and communication technology from the Sapienza University of Rome, Rome, Italy, in 2017 and 2021, respectively.

She was a Visiting Researcher with Stiching imec, Eindhoven, The Netherlands, from April 2019 to September 2019. She is currently a Researcher and a Marie Curie Fellow with the Institut d'Électronique et des Technologies du numéRique/French National Center for Scientific Research (CNRS), Rennes, France. Her research interests include the field of innovative biomedical applications of electromagnetic fields and radars for vital signs monitoring.

Dr. Sacco was a recipient of the 2022 Antennas and Propagation Society (AP-S) Fellowship, the "Bourse de Jeunes Chercheurs" Grant at XXXIV General Assembly and Scientific Symposium (GASS) of the International Union of Radio Science (Union Radio Scientifique Internationale-URSI) 2021, the Best Student Paper Award at the XXXIII General Assembly and Scientific Symposium (GASS) of the International Union of Radio Science (Union Radio Scientifique Internationale-URSI) 2020, and the Best Student Paper Award at Photonics & Electromagnetics Research Symposium (PIERS) 2019.

MAXIM ZHADOBOV (Senior Member, IEEE) received the Ph.D. and Habilitation á Diriger des Recherches degrees from the Institut d'Electronique et des Technologies du numéRique (IETR), University of Rennes 1, Rennes, France, in 2006 and 2016, respectively.

He was a Postdoctoral Researcher with the Center for Biomedical Physics, Temple University, Philadelphia, PA, USA, until 2008, and then joined the French National Center for Scientific Research (CNRS). He is currently a Senior Research Scientist with the IETR/CNRS in charge of the Electromagnetic Waves in Complex Media (eWAVES) Research Group. He was also on review boards of more than 15 international journals and conferences, and has been acting as an expert at research councils worldwide. He has coauthored five book chapters, 85 research articles in peer-reviewed international journals, and more than 200 contributions to conferences and workshops. His review article in the *International Journal of Microwave and Wireless Technologies* was the most cited paper, from 2016 to 2020. A paper published by his research group, in 2019, is in journal Top 100 of *Scientific Reports* (Nature). He has been involved in 26 research projects (14 as a PI). His research interests include innovative biomedical applications of electromagnetic fields and associated technologies.

Dr. Zhadobov was a TPC Member and/or a Session Organizer at international conferences, including EUMW 2022, IEEE IMBioC 2022, AT-AP-RASC 2022, BioEM 2019, EuMW 2019, IEEE iWEM 2017, MobiHealth 2015–2017, BodyNets 2016, and IMWS-Bio 2014. He was an Elected Member of EBEA Council, from 2017 to 2021. He is a member of IEEE TC95.4. He was a recipient of the CNRS Medal in 2018, the EBEA Award for Excellence in Bioelectromagnetics in 2015, and Brittany's Young Scientist Award, in 2010. Since 2010, the Ph.D. students he worked with have been recipients of seven national scientific awards and six awards from the Bioelectromagnetics Society, URSI, IEEE Antennas and Propagation Society, and IEEE Microwave Theory and Technology Society. He was the TPC Co-Chair of BioEM 2021/2020. He is the Vice-President of URSI France Commission K. He is an Associate Editor of IEEE JOURNAL OF ELECTROMAGNETICS, RF AND MICROWAVES IN MEDICINE AND BIOLOGY and served as a Guest Editor for several special issues, including Human Exposure in 5G and 6G Scenarios of *Applied Sciences* and Advanced Electromagnetic Biosensors for Medical, Environmental and Industrial Applications of *Sensors*.

WALID EL HAJJ (Member, IEEE) received the National Degree of Master for his research in microwave materials and devices for communication systems and the Ph.D. degree in information and communications sciences and technologies from Telecom Bretagne, Brest, France, in 2008 and 2011, respectively.

From 2011 to 2013, he was a Researcher with the Department of Microwave, Lab-STICC/MOM Laboratory, Telecom Bretagne. He joined Intel Corporation, in 2014. He is currently a Scientist Officer with the Wireless Test and Certification Center Group. He is also leading the different research and development activities related to new wireless technologies and products certification. He is participating and leading several standardization efforts in the human exposure and product safety domain. He is mandated as an Expert of the French Standardization Association (AFNOR). Since 2017, he has been participating in the development of several IEEE/IEC standards on human exposure computational and measurement assessments. He is also the Co-Convener of IEC/IEEE JWG12 developing measurement methods standards to assess the power density in close proximity to the head and body from 6–300 GHz.

Dr. El Hajj is a member of IEC TC 106 and IEEE ICES TC95. He is also a member of CMC TF Radio Group in IECEE. He was the Chair of WG 5 under SC 6 of IEEE ICES TC95 that published the guide IEEE 2889-2021 studying the different aspects of incident power density definition publishing.

AKIMASA HIRATA (Fellow, IEEE) received the B.E. and M.E. degrees in communications engineering from Osaka University, Suita, Japan, in 1996, 1998, and 2000, respectively.

From 1999 to 2001, he was a Research Fellow of the Japan Society for the Promotion of Science. He was also a Visiting Research Scientist at the University of Victoria, Victoria, BC, Canada, in 2000. In 2001, he joined the Department of Communications Engineering, Osaka University, as an Assistant Professor. In 2004, he joined the Department of Computer Science and Engineering, Nagoya Institute of Technology, as an Associate Professor, where he is currently a Full Professor. His research interests include electromagnetic safety, risk management system for heat-related illness, methods in neuroscience, antennas, filters, and related computational techniques.

Prof. Hirata is a fellow of the Institute of Physics and a member of IEICE, IEE Japan, and Bioelectromagnetics Society. He received several awards, including the Young Scientists' Prize (2006) and Prizes for Science and Technology (Research Category, in 2011, Public Understanding Promotion Category, in 2014 and 2020) by the Commendation for Science and Technology by the Minister of Education, Culture, Sports, Science, and Technology, Japan, and IEEE EMC-S Technical Achievement Award, in 2015; the Japan Academy Medal and JSPS Prize, in 2018; and the Japan Open Innovation Prize (President of the Science Council of Japan Prize, in 2022) from the Cabinet Office. He is an Editorial Board Member of *Physics in Medicine and Biology*, a member of the Main Commission, the Chair of Project Group of International Commission on Non-Ionizing Radiation Protection, a member of the Administrative Committee and a Subcommittee (EMF Dosimetry Modeling) Chair of IEEE International Committee on Electromagnetic Safety, and an Expert of World Health Organization. From 2006 to 2012, he was also an Associate Editor of the IEEE TRANSACTIONS ON BIOMEDICAL ENGINEERING.